ISSN 0915-633X

NATIONAL INSTITUTE FOR FUSION SCIENCE

Classification of Particle Orbits near the Magnetic Axis in a Tokamak by Using Constants of Motion

S. Satake, H. Sugama, M. Okamoto and M. Wakatani

(Received - Dec. 5, 2000)

NIFS-677 Jan. 2001

RESEARCH REPORT
NIFS Series

TOKI, JAPAN

Classification of particle orbits near the magnetic axis in a tokamak by using constants of motion

Shinsuke Satake†, Hideo Sugama‡, Masao Okamoto‡and Masahiro Wakatani§

† Department of Fusion Science, The Graduate University for Advanced Studies,
Toki, Gifu, 509-5292, Japan
‡ National Institute for Fusion Science, Toki, Gifu, 509-5292, Japan
§Graduate School of Energy Science, Kyoto University, Uji, Kyoto, 611-0011, Japan

E-mail: satake@nifs.ac.jp

Abstract. A classification of particle orbits near the magnetic axis in a tokamak is presented in a space of constants of motion (COM), which is important to apply Lagrangian formulation of neoclassical transport theory to the region near the axis. Orbit types are distinguished by the number of the turning points of $\sigma_\parallel = v_\parallel/|v_\parallel|$ and $\sigma_\theta = \theta/|\dot{\theta}|$ on each orbit, where $v_\parallel$ is the velocity parallel to the magnetic field, and $\dot{\theta}$ is the poloidal angular velocity. As a set of COM, $(\mathcal{E}, \mu, \langle r \rangle)$ is taken, where $\mathcal{E}$ is the energy of a particle, μ is the magnetic moment, and $\langle r \rangle$ is the bounce-averaged minor radius position of a particle orbit. Compared with a familiar set of COM (v, ξ_s, r_s), where v is the particle velocity, r_s is the minor radius at which an orbit crosses the mid-plane, and $\xi_s = v_\parallel/v$ evaluated at the crossing point, the set of COM $(\mathcal{E}, \mu, \langle r \rangle)$ is more suitable in practice for Lagrangian formulation of neoclassical transport theory, in which the particle diffusion is described by the change of average position of particles $\langle r \rangle$ by collisions. Near the magnetic axis, it is found that there are overlaps in regions of orbit types in the $(\mathcal{E}, \mu, \langle r \rangle)$ space and that $\langle r \rangle$ has a minimum value for a given $\mathcal{E}$.

PACS numbers: 52.20 Dq, 52.25 Fi

Keywords: particle orbit, neoclassical transport theory

1. Introduction

There have been many works which consider neoclassical transport near the magnetic axis in tokamaks. It is to be noted that particle orbits passing near the axis are different from those predicted by the conventional analysis which is valid away from the axis. For example, a radial width of a trapped particle, or a "banana width", is approximated in the conventional analysis as

$$\Delta_b = 2\sqrt{\epsilon}\rho_p, \tag{1}$$

where $\epsilon = r/R$ is the inverse aspect ratio and $\rho_p = mv/eB_p$ is the poloidal Larmor radius. (MKS units are used in this paper.) The fraction of trapped particles is given as

$$f_t = \sqrt{2\epsilon}. \tag{2}$$

These characteristic quantities can be written by local values such as ϵ and ρ_p when an instant radial position of a particle r is assumed to be much larger than the banana width of the orbit Δ_b; $\Delta_b/r \ll 1$. However, approaching the magnetic axis, a banana width increases because $\rho_p \propto 1/B_p \propto 1/r$. Therefore, equations (1) and (2) are not valid near the axis. Actually, both the banana width and the fraction of banana particles are finite on the magnetic axis as found by Stix [1]. The typical orbit width of trapped particles passing near the magnetic axis, which are called "potato" particles [2], is $\sim (q^2\rho^2 R_0)$, where q is the safety factor, $\rho = mv/eB_0$ is the gyroradius, and R_0 is the major radius of the magnetic axis.

Detailed investigation about the properties of particle orbits is the basis for neoclassical transport theory. To make a classification of orbit types near the magnetic axis, we introduce two signs with respect to particle motions;

$$\sigma_\parallel \equiv \frac{v_\parallel}{|v_\parallel|}, \tag{3}$$

$$\sigma_\theta \equiv \frac{\dot{\theta}}{|\dot{\theta}|}, \tag{4}$$

where $v_\parallel$ is the velocity component parallel to the magnetic field. The poloidal angular velocity $\dot{\theta}$ is defined as

$$\dot{\theta} \equiv \mathbf{v}\cdot\nabla\theta = (\mathbf{v}_\parallel + \mathbf{v}_d)\cdot\nabla\theta, \tag{5}$$

where $\mathbf{v}_d$ is the sum of the grad-B and curvature drift velocity. Conventionally, orbit topology is classified as "passing" or "trapped" depending on whether the sign of parallel velocity $\sigma_\parallel$ reverses along an orbit or not. However, particle orbits passing near the magnetic axis are strongly affected by grad-B and curvature drift, and there appear new types of orbit.

One of the new types of orbit has two turning points of σ_θ but has no turning points of $\sigma_\parallel$. As shown later, such orbits appear on the outside or the inside of the magnetic axis. We call them "outer-circulating" and "inner-circulating" orbits to distinguish them from passing orbits which encircle the axis. Whether a circulating particle is located on the inside or the outside of torus is determined by the sign $\sigma_\parallel$. There exists the other type of orbit which encircle the magnetic axis and have two turning points of $\sigma_\parallel$. This orbit is called "kidney". We show in the paper that all these orbit types can be properly classified by counting the number of turning points of both $\sigma_\parallel$ and σ_θ.

Shaing *et al* [3, 4], Helander [5], and Lin *et al* [6] have attempted to extend the neoclassical transport theory to the region near the axis by taking account of potato particles. These studies are based on Eulerian representation of transport equations. However, it has been noticed that Lagrangian formulation of transport theory [7, 8, 9] is more suitable to treat non-local nature of the neoclassical transport, such as the effects of large banana width, in the banana regime. Lagrangian formulation is constructed by transforming the independent variables of the Fokker-Planck equation in Cartesian coordinates (x_i, v_i) $(i = 1,2,3)$ to three constants of motion (COM) (C_1, C_2, C_3) in axisymmetric systems and the other three variables (z_1, z_2, z_3) describing fast motion of particles. One can choose an arbitrary set of COM (C_1, C_2, C_3). However, to obtain a suitable transport equation, C_1 and C_2 must be velocity-like variables, while C_3 must be related to a radial coordinate, as remarked by Bernstein [7]. In Lagrangian formulation, transport processes are described by slow diffusion of COM by collisions. Transport equation is obtained by averaging the Fokker-Planck equation by z_i and then taking the moment over C_1 and C_2. The particle transport equation is given in the form

$$\frac{\partial n_3}{\partial t} + \frac{\partial}{\partial C_3}\Gamma(C_3) = 0, \tag{6}$$

where n_3 is the particle number per unit C_3 and the second term describes the particle flux. Γ is expressed by the sum of the products of the transport coefficients $I_i(C_3)$ and driving forces as follows,

$$\Gamma(C_3) = I_1\frac{d}{dC_3}\ln n_3 + I_2\frac{d}{dC_3}\ln T + I_3\frac{d}{dC_3}\Phi, \tag{7}$$

where T is the temperature of the plasma and Φ is the potential. The thermal flux can be given by similar equations like (6) and (7).

A familiar choice of COM, which is often used to classify orbit types, is $(C_1, C_2, C_3) = (v, \xi_s, r_s)$, where v is the particle velocity, r_s is the minor-radius at which the orbit crosses the mid-plane $Z = 0$, and $\xi_s = v_\parallel/|v_\parallel|$ is the cosine of the pitch angle at that point. To estimate the transport coefficients in the banana regime, one must know the trapped particle region in the (v, ξ_s, r_s) space, which has been investigated by Chu [10] and Egedal [11]. In the present paper, a simple analytic expression of the boundary for each type of orbit is given. As shown in section 3.1, classification of orbit in the (v, ξ_s, r_s) space is rather complicated near the magnetic axis. Moreover, because any particle cross the mid-plane twice, there are a pair of points (v, ξ_s, r_s) which correspond to one orbit. Therefore, the physical meaning of the flux expressed by equation (6) with $C_3 = r_s$ becomes ambiguous near the magnetic axis, where the typical orbit width (difference between two values of r_s for each orbit) is wide.

Another choice of COM is $(\mathcal{E}, \mu, \langle r \rangle)$ used by Wang [9], where $\mathcal{E}$ is the particle energy, μ is the magnetic moment, and $\langle r \rangle$ is the bounce-averaged radial position of a particle. Particle transport is described by the diffusion of average radial position of orbits by collisions. Then this description is physically more understandable than that in the former choice of COM. In the $(\mathcal{E}, \mu, \langle r \rangle)$ space, the distinction between passing orbits and inner- and outer-circulating orbits, as well as the distinction between $\sigma_\parallel$ and σ_θ becomes important.

In the limit of zero-banana-width approximation, in which we assume $r_s \simeq \langle r \rangle \simeq r$, neoclassical transport equations obtained by Lagrangian formulation agree with those obtained by conventional Eulerian formulation [12]. Then it is interesting to apply the Lagrangian formulation to the region near the magnetic axis where the effect of finite orbit width is really important. In the present paper, we make a clear classification of orbit types near the magnetic axis with two sets of COM variables $(C_1, C_2, C_3) = (v, \xi_s, r_s)$ and $(\mathcal{E}, \mu, \langle r \rangle)$ and compare these two representations. The classification is the basis to extend the neoclassical transport theory by Lagrangian formulation to the region near the axis.

The remainder of the paper is organized as follows. In section 2, we analyze particle orbits using the guiding-center equations of motion and three constants of motion in an axisymmetric system, and classify orbit types in terms of σ_θ and $\sigma_\parallel$. The region of each type of orbit is shown in the (v, ξ_s, r_s) space and in the $(\mathcal{E}, \mu, \langle r \rangle)$ space in section 3. The results of the paper are summarized in section 4.

2. Particle orbits

Let us consider an axisymmetric configuration like a tokamak. Coordinates are chosen as in figure 1; r is the minor radius, ζ the toroidal angle, and θ the poloidal angle. A general axisymmetric magnetic field is written as $\mathbf{B} = I\nabla\zeta + \nabla\zeta \times \nabla\psi$, where $I = RB_t$ and ψ is the poloidal flux. For simplicity, we assume that the magnetic surfaces have concentric circular poloidal cross sections and that the safety factor q is constant near the magnetic axis. Then the poloidal flux can be written as $\psi = (B_0 r^2)/(2q)$, where $B_0 = I/R_0$ is the magnetic field strength at the magnetic axis $R = R_0$. Note that we take $\mathbf{j} \cdot \mathbf{B} > 0$, where $\mathbf{j}$ is the plasma current density. In an axisymmetric system, there are three constants of motion; $\mathcal{E} = mv^2/2 + e\Phi$ is the total energy of a particle, $\mu = mv_\perp^2/2B$ is the magnetic moment, and $P_\zeta = \psi - Iv_\parallel/\Omega$ is the toroidal canonical momentum. Here, Φ is the electrostatic potential and $\Omega = eB/m$ is the gyrofrequency. We assume that the variation of the potential over an orbit is negligible compared with $\mathcal{E}$,

$$e\Delta_r \left| \frac{d\Phi}{dr} \right| \ll \mathcal{E},$$

where Δ_r represents a characteristic orbit width.

Particle motion averaged with respect to gyrophase is described by the guiding-center equations of motion. To the lowest order in ρ/L, where ρ is the gyroradius and L the gradient scale length of the magnetic field, they are written as

$$\mathbf{v} = v_\parallel \hat{b} + \frac{\hat{b}}{m\Omega} \times (\mu \nabla B + m v_\parallel^2 \hat{b} \cdot \nabla \hat{b}), \tag{8}$$

$$\frac{dv_\parallel}{dt} = -\frac{\mu}{m} \hat{b} \cdot \nabla B, \tag{9}$$

where $\hat{b}$ is the unit vector parallel to the magnetic field. The second term on the right-hand side of equation (8) represents the drift velocity $\mathbf{v}_d$. Using the large-aspect-ratio and low-β approximations, we can write

$$B \simeq \frac{B_0}{1 + \epsilon \cos\theta} \simeq B_0(1 - \epsilon \cos\theta),$$

$$\mathbf{v}_d \simeq -\frac{1}{R_0 \Omega_0} \left(v_\parallel^2 + \frac{1}{2} v_\perp^2 \right) \hat{z},$$

where $\Omega_0 = eB_0/m$. From these expressions, the poloidal angular velocity is written as

$$\dot{\theta} \equiv \mathbf{v} \cdot \nabla\theta = \frac{1}{qR_0} \left[v_\parallel - \frac{q}{r\Omega_0} \left(v_\parallel^2 + \frac{1}{2} v_\perp^2 \right) \cos\theta \right], \tag{10}$$

which shows that the contribution of $\mathbf{v}_d$ to $\dot{\theta}$ increases proportional to $1/r$ near the magnetic

axis. Particle orbits can be analyzed with the three constants of motion and equations (8) – (10).

Examples of orbits near the axis numerically calculated by equations (8) and (9) are shown in figures 2 – 5. In these figures, orbits of hydrogen ions with $\mathcal{E} = 10\text{keV}$ are plotted, where other parameters are given as $R_0 = 4\text{m}$, $q = 3$, $B_0 = 4\text{T}$. The arrows in these figures represent the direction of the particle motion. In the calculations, the minor radius of the starting point r_s on the mid-plane $Z = 0$ and the cosine of the pitch angle of velocity at that point $\xi_s = v_\parallel/v$ are given as initial conditions. Orbit types are classified in this paper according to the number of turning points of $\sigma_\parallel$ and σ_θ defined in equations (3) and (4), respectively.

Figure 2 shows the orbits of passing particles. Both the signs $\sigma_\parallel$ and σ_θ are constant over the orbits. The radial displacement of a passing orbit ($|r(\theta = 0) - r(\theta = \pi)|$) has a minimum value for the particles with $\xi_s = \pm 1$, as in the orbits B and D. Note that $v_\parallel$ is constant for such particles because $\mu = 0$ in equation (9). From the equation of conservation of P_ζ, one can find the minimum displacement is $2q\rho$. On the other hand, A and C are the passing orbits which have the maximum radial displacement starting from the same positions as in B and D. As shown later in figure 6, these particles are on the boundary to other types of orbit. Though the maximum displacement of passing orbit near the axis becomes as large as $(q^2\rho^2 R_0)^{1/3}$, most of passing particles still have a small displacement of the order of $2q\rho$.

Figure 3 shows banana orbits. We identify banana orbits with those which have two turning points for each of $\sigma_\parallel$ and σ_θ, and then do not encircle the magnetic axis. The banana width, which is measured on the mid-plane, increases when the orbit is close to the magnetic axis, but it remains finite even if the orbit passes through the axis. The orbit E in figure 3 represents the widest banana orbit. To obtain the maximum banana width, let us consider a particle which starts from the magnetic axis $r_s = 0$ with $\xi_0 = v_{\parallel 0}/v < 0$. If the particle has the turning point at $(r, \theta) = (r_1, \pi)$, then $\dot{\theta} = 0$ on that point. Therefore, from equation (10), we obtain

$$r_1 = -\frac{q}{v_{\parallel 1}\Omega_0}\left(v_{\parallel 1}^2 + \frac{1}{2}v_{\perp 1}^2\right) \simeq -\frac{q}{v_{\parallel 1}\Omega_0}\frac{\mu B_0}{m}\left(1 + \frac{r_1}{R_0}\right). \tag{11}$$

where $v_{\parallel 1}$ and $v_{\perp 1}$ are the parallel and perpendicular velocities at $r = r_1$ respectively, and we use an approximation $v_{\parallel 1}^2 \ll v_{\perp 1}^2$ at the turning point. On the other hand, from the conservation of $\mathcal{E}$ and P_ζ at $r = 0$ and r_1, we have

$$\frac{v_{\parallel 0}^2}{2} + \frac{\mu B_0}{m} = \frac{v_{\parallel 1}}{2} + \frac{\mu B_0}{m}\left(1 + \frac{r_1}{R_0}\right), \tag{12}$$

$$v_{\parallel 0} = v_{\parallel 1} - \frac{\Omega_0 r_1^2}{2qR_0}. \tag{13}$$

Solving equations (11) – (13), we obtain

$$r_1 = (2q^2\rho^2 R_0)^{1/3}, \tag{14}$$

$$\xi_0 = -\frac{3}{2}\left(\frac{q\rho}{2R_0}\right)^{1/3}. \tag{15}$$

Note that we take $\rho = v/\Omega_0$ here and hereafter. Solving similar equations for constants of motion concerning $(r, \theta) = (r_1, \pi)$ and $(\Delta_{bmax}, 0)$, we obtain the maximum banana width Δ_{bmax},

$$\Delta_{bmax} = 2(2q^2\rho^2 R_0)^{1/3} = 2r_1. \tag{16}$$

Lin, Tang, and Lee [6] showed a similar result, but it has different numerical factors. It is because they used $v_{\parallel 1} = 0$ as the condition of the turning point on the poloidal cross section. Since the positions of $v_\parallel = 0$ and $\dot{\theta} = 0$ tend to deviate from each other on banana orbits passing near the magnetic axis, using $\dot{\theta} = 0$ as the poloidal turning condition is correct.

Figure 4 shows circulating orbits. Circulating particles have the constant $\sigma_\parallel$ but σ_θ changes twice on the orbits. They are located on the inside or the outside of the torus. In the case of ion, $\sigma_\parallel = +1$ for outer-circulating (solid lines) and $\sigma_\parallel = -1$ for inner-circulating (dashed lines). Note that this criterion is reversed for electrons, or when the direction of the parallel current is antiparallel to the magnetic field. The maximum width of outer-circulating orbit Δ_{ocmax} can be obtained by solving the equations of motion for the particle with $(r_s, \xi_s) = (0, 0)$, which corresponds to the orbit G. The result is

$$\Delta_{ocmax} = (4q^2\rho^2 R_0)^{1/3}. \tag{17}$$

On the other hand, the widest inner-circulating orbit H corresponds to the inner part of the widest banana orbit E in figure 3. Thus we obtain

$$\Delta_{icmax} = r_1 = (2q^2\rho^2 R_0)^{1/3}. \tag{18}$$

The minimum width of circulating orbits is zero. Such particles satisfy $\dot{\theta} = 0$ and $\dot{r} = 0$ on the mid-plane, and move only in the toroidal direction. From equation (10), this condition is written as

$$r_s = \frac{q\rho}{2\xi_s}(1 + \xi_s^2), \tag{19}$$

where the domain of r_s is extended to negative values, and $r_s < 0$ represents the starting point of a inner-circulating orbit $(r, \theta) = (|r_s|, \pi)$.

A remarkable difference between outer- and inner-circulating orbits is the region in which each type of orbit can exist. Like the orbit J, inner-circulating orbits can exist only in the region $-\Delta_{icmax} \leq r_s \leq 0$ enclosed by the widest one; the orbit H. On the other hand, outer-circulating orbits can exist away from the axis $r_s \geq \Delta_{ocmax}$ like the orbit I. Orbits like I are conventionally classified as "deeply-trapped" banana, but in fact they have no turning point of $\sigma_{\|}$.

Figure 5 shows orbits which encircle the magnetic axis but $\sigma_{\|}$ changes twice on these orbits. We divide these orbits further into two types. One type consists of the orbits which have four turning points of σ_θ like the orbit L in figure 5. The other consists of the orbits which have no turning point of σ_θ like the orbit M. We name the former "concave-kidney" to distinguish it from the latter called "kidney" by Chu [10]. Concave-kidney orbits have a larger radial displacement than kidney orbits.

The summary of the classification of orbits is shown in Table I. Orbits are clearly classified by the number of turning points of $\sigma_{\|}$ and σ_θ. One can see that all the orbits which cannot encircle the magnetic axis (banana and circulating orbits) have two turning points of σ_θ.

3. Classification of orbit types by constants of motion

3.1. Classification in (v, ξ_s, r_s) space

In this subsection, we classify orbit types in the (v, ξ_s, r_s) space, where r_s and ξ_s is defined in section 2. This set of COM is often used to classify orbit types, and a similar set of COM is used in Lagrangian formulation of transport theory by Zaitsev *et al* [8].

The regions and the boundaries in the (r_s, ξ_s) plane for each type of orbit of ions with $\mathcal{E} = 10$keV in the model configuration used in section 2 are shown in figure 6, and the regions near the origin and near the concave-kidney region are magnified in figures 7 and 8, respectively. We follows the way of showing orbit regions by Egedal [11], and negative r_s means the crossing points of particle orbits on the mid-plane $Z = 0$ at the inside of the torus; $(r, \theta) = (|r_s|, \pi)$. The points (r_s, ξ_s) which correspond to the orbits A to M in figures 2 – 5 are plotted in figures 6 – 8. Note that there are two different points in the (r_s, ξ_s) plane corresponding to the same orbit, because any orbit crosses the mid-plane twice. In figure 6, the points E, G and H correspond to orbits with maximum width of banana Δ_{bmax}, outer-circulating Δ_{ocmax}, and inner-circulating Δ_{icmax}, respectively. We newly distinguish the region of concave-kidney (vi) from the region kidney (v). This distinction becomes important in the next subsection in which orbits are classified in $(\mathcal{E}, \mu, \langle r \rangle)$ variables.

Though Egedal have shown a method to obtain boundaries in general configurations, it is still useful to give simple expressions for boundaries in the model configuration used here. Dotted lines in the circulating regions in figure 6 correspond to the orbits stagnated at r_s given by equation (19) and $Z = 0$. The other boundaries are given as follows.

First, the boundary *b1* which lies between the outer-circulating and co-passing region and between the inner-circulating and counter-passing regions is obtained from equations like (12) and (13) for a particle passing through the magnetic axis. The result is

$$\xi_s = \frac{1}{2}\left[\frac{R_0}{q\rho}\epsilon_s(1+2\epsilon_s) \pm\sqrt{\left(\frac{R_0}{q\rho}\right)^2\epsilon_s^2(1+3\epsilon_s+3\epsilon_s^2)-4(1+2\epsilon_s)}\right], \tag{20}$$

where $\epsilon_s = r_s/R_0$ and we choose $-$ for $2q\rho \leq r_s \leq \Delta_{ocmax}$ (the boundary of the outer-circulating region) and $+$ for $-\Delta_{icmax} < r_s < -2q\rho$ (the boundary of the inner-circulating region). This equation also represents the boundary between the banana and concave-kidney regions E-G at $\Delta_{ocmax} < r_s < \Delta_{bmax}$.

Second, to obtain the boundaries between the concave-kidney and kidney regions G-X in figures 6 and 8, let us consider a concave-kidney particle which starts from the point $(r, Z) = (r_s, 0)$ and turns at (r_t, θ_t). The equations of the constants of motion are written as

$$\frac{v_{\|s}^2}{2} + \frac{\mu B_0}{m}(1-\epsilon_s) = \frac{v_{\|t}^2}{2} + \frac{\mu B_0}{m}(1-\epsilon_t\cos\theta_t), \tag{21}$$

$$v_{\|s} - \frac{\Omega_0 r_s^2}{2qR_0} = v_{\|t} - \frac{\Omega_0 r_t^2}{2qR_0}, \tag{22}$$

where the subscripts s and t mean the values at the points $r = r_s$ and r_t respectively. From the condition $\dot{\theta} = 0$ at (r_t, θ_t), we obtain

$$\cos\theta_t = \frac{2r_t\xi_t}{q\rho(1+\xi_t^2)} \quad (<0). \tag{23}$$

Combining equations (21) – (23), we obtain

$$-\left(\frac{1-\epsilon_s}{1-\xi_s^2}\right)\xi_t^4+3\xi_t^2-4\left(\xi_s-\frac{R_0}{2q\rho}\epsilon_s^2\right)\xi_t + \frac{(\xi_s^2-\epsilon_s)}{(1-\xi_s^2)}=0. \quad (24)$$

The necessary condition for a concave-kidney particle to exist is that equation (24) has a real solution for ξ_t. Therefore, the boundaries G-X in the (r_s,ξ_s) plane are approximately given by the discriminant of equation (24) (neglecting $O(\xi_t^4)$ term),

$$D=4\left(\xi_s-\frac{R_0}{2q\rho}\epsilon_s^2\right)^2-\frac{3(\xi_s^2-\epsilon_s)}{(1-\xi_s^2)}=0. \quad (25)$$

Third, solving equations for a particle which passes the mid-plane $Z=0$ with $\xi=0$, we obtain

$$\xi_s^3-2\epsilon_s(1-\epsilon_s)\xi_s+\frac{2q\rho}{R_0}=0. \quad (26)$$

This equation, which corresponds to the boundary *b2* in figures 6 and 8, has two real solutions $\xi_s>0$ in the region $r_s \geq 1.5(q^2\rho^2R_0)^{1/3}$. One solution represents the boundary between the banana and outer-circulating regions, while the other corresponds to the boundary between the kidney and passing regions. As shown in figure 8, the kidney region is very narrow and then the latter solution is almost the same as the upper boundary of the banana region *b3* at $r_s>\Delta_{bmax}$. In particular, away from the magnetic axis, two solutions of equation (26) are approximated as $\xi_s \simeq q\rho/r_s \sim 0$ and $\xi_s \simeq \sqrt{2\epsilon_s}$, which give the conventional representation of the banana region.

Finally, the upper and lower boundaries of the banana region *b3* are obtained from equations for a particle which has the turning point $\dot{\theta}=0$ at $(r_t,\theta_t=\pi)$. Taking $r_t=x\Delta_{icmax}$ $(x\geq 1)$ and using the approximation $r_t/R_0 \ll 1$, these boundaries (r_s,ξ_s) can be given in terms of x as

$$\begin{cases} r_s=x(1\pm x^{-3/2})\Delta_{icmax}, \\ \xi_s=\left(\dfrac{q\rho}{2R_0}\right)^{1/3}\left(\pm 2x^{1/2}+\dfrac{1}{2x}\right), \end{cases} \quad (27)$$

where we choose + (−) for the upper (lower) boundary. When $x\gg 1$, these equations result in $\xi_s \simeq \pm\sqrt{2\epsilon_s}$. Applying these equations to $x<1$, they represent the boundary E-X in figures 6 and 8. In figure 6, three boundaries, which are given by equations (19), (25), and (27), respectively, converge on the point X at $r_s<0$. This point is given by solving equation (27) for $|r_s|=r_t$ as

$$[r_s,\xi_s]=\left[-\left(\frac{q^2\rho^2R_0}{2}\right)^{1/3},-\left(\frac{q\rho}{4R_0}\right)^{1/3}\right], \quad (28)$$

and the other pair of the point X at $r_s>0$ is written as

$$[r_s,\xi_s]=\left[3\left(\frac{q^2\rho^2R_0}{2}\right)^{1/3},\frac{3}{2}\left(\frac{2q\rho}{R_0}\right)^{1/3}\right]. \quad (29)$$

Let us discuss the results of this subsection. As shown in equation (15), the banana region have the finite fraction $|\xi_0|$ (~ 0.16 for the parameters used in figures 2 – 5) at the magnetic axis. We can see from figure 6 that a considerable fraction of particles which have been regarded as bananas are actually identified as outer-circulating particles. Within $r<\Delta_*\equiv 2q\rho$ ($\sim$ 2cm), nearly half of particles are circulating ones. The deviation of the banana-passing boundary from the conventional expression in equation (2) is significant for $r<\Delta_{bmax}$ ($\sim$ 20cm). Since ξ_0, Δ_* and Δ_{bmax} increases with $q\rho$, the modification on orbit classification is significant for high energy particles and in high q-value configurations. It is also noted that because $\rho_e/\rho_i \propto \sqrt{m_e/m_i} \ll 1$ for the two species with the same energy, the modification on the particle orbits near the axis is more significant for ions than that for electrons.

Recently, neoclassical transport theory has been extended by taking account of potato particles. Potato particles are defined by Porcelli *et al* [2] as those which have the typical orbit width $\Delta_r \sim (q^2\rho^2R_0)^{1/3}$. In the (r_s,ξ_s) plane, we find that any particle which has one of a pair of points (r_s,ξ_s) around the origin in the range about $|r_s| \leq (q^2\rho^2R_0/2)^{1/3}$ and $|\xi_s| \leq (q\rho/R_0)^{1/3}$ has this characteristic orbit width. Therefore, potato orbits are not only banana orbits passing through near the magnetic axis but consist of many types of orbit appearing around the origin in the (r_s,ξ_s) plane in figure 6, and all of them will contribute to the neoclassical transport near the axis.

There are some difficulties in using the set of COM (v,ξ_s,r_s) for Lagrangian transport theory in practice. The position r_s jumps when a particle changes from passing to banana particle, and from inner-circulating to concave-kidney particles. Such a discontinuity is unfavorable to construct transport equations. Moreover, since there are two values of r_s for each orbit and the difference between them is large for potato particles, the transport equation in the form like equation (6) is not simply connected to the transport phenomena in real space if C_3 is taken as r_s. Though the classification of orbit types in the (v,ξ_s,r_s) space is a useful way in itself, it seems not to be suitable to apply Lagrangian formulation in the (v,ξ_s,r_s) space to the region near the magnetic

axis.

3.2. Classification in $(\mathcal{E}, \mu, \langle r \rangle)$ space

Let us consider a transformation from Cartesian coordinate system (x_i, v_i) to $(C_i, z_i) = (\mathcal{E}, \mu, \langle r \rangle, \theta, \zeta, \phi)$. In axisymmetric systems with drift approximation, the toroidal angle ζ and the gyrophase ϕ can be neglected, and the guiding-center position is described by the minor radius r and the poloidal angle θ. Three constants of motion are defined as

$$\mathcal{E} \equiv \frac{1}{2}mv^2 + e\Phi, \tag{30}$$

$$\mu \equiv \frac{mv_\perp^2}{2B}, \tag{31}$$

$$\langle r \rangle \equiv \frac{1}{\tau_b} \oint r \frac{d\theta}{\dot{\theta}}, \tag{32}$$

where $v_\perp$ is the velocity perpendicular to the magnetic field lines, and the integral in equation (32) is carried out along one poloidal circuit of an orbit. The poloidal bounce time τ_b is given by

$$\tau_b = \oint \frac{d\theta}{\dot{\theta}}. \tag{33}$$

We can also use ψ and $\langle \psi \rangle$ instead of r and $\langle r \rangle$ for a radial coordinate as in the work by Wang [9], when it is convenient.

Note that the definition of the orbital integral is different according to orbit types. For passing orbits and kidney orbits, θ varies monotonously in time. Then the orbital integral of a function $F(r, \theta)$ along these orbits is defined as

$$\oint F(r,\theta) d\theta = \sigma_\theta \int_0^{2\pi} F(r,\theta) d\theta, \tag{34}$$

where r is a function of $(\mathcal{E}, \mu, \langle r \rangle, \theta)$ and depends on orbit types. On the other hand, as shown in section 3.1, banana, outer-circulating, and inner-circulating orbits have two turning points of σ_θ at which $\dot{\theta} = 0$. Writing one of the turning points $\theta = \theta_t$ $(0 \le \theta_t \le \pi)$, the orbital integral is defined as

$$\oint F(r,\theta) d\theta = \sum_{\sigma_\theta = \pm 1} \sigma_\theta \int_{-\theta_t}^{+\theta_t} F(r,\theta) d\theta \tag{35}$$

for banana and outer-circulating orbits, and

$$\oint F(r,\theta) d\theta = \sum_{\sigma_\theta = \pm 1} \sigma_\theta \int_{\theta_t}^{2\pi - \theta_t} F(r,\theta) d\theta \tag{36}$$

for inner-circulating orbits. Note that the integrand F depends on the sign σ_θ through $r = r(C_i, \theta; \sigma_\theta)$ as shown in figure 9, where σ_θ (not $\sigma_\parallel$) indicates the inner or outer part of a circulating (or a banana) orbit. For concave-kidney orbits, the definition is more complicated. As shown in figure 10, there are four turning points $\theta = \pm\theta_{t1}, \pm\theta_{t2}$ $(\pi/2 \le \theta_{t2} \le \theta_{t1} \le \pi)$ at which $\dot{\theta} = 0$. Therefore the orbital integral is defined as

$$\oint d\theta = \sigma_\theta(\theta = 0) \cdot \left[\int_{-\theta_{t1}}^{\theta_{t1}} d\theta + \int_{\theta_{t1}}^{\theta_{t2}} d\theta + \int_{\theta_{t2}}^{2\pi - \theta_{t2}} d\theta + \int_{2\pi - \theta_{t2}}^{2\pi - \theta_{t1}} d\theta \right], \tag{37}$$

where $\sigma_\theta(\theta = 0)$ is $+1$ for ions and -1 for electrons in the present configuration.

Next, let us show the region of each orbit types in the $(\mathcal{E}, \mu, \langle r \rangle)$ space. Here, introduce the normalized magnetic moment λ_0 as

$$\lambda_0 \equiv \frac{\mu B_0}{\mathcal{E}}. \tag{38}$$

In figure 11, we classify the orbit types in the $(\langle r \rangle, \lambda_0)$ plane for hydrogen ions with $\mathcal{E} = 10$keV, where the configuration is set the same as in section 3.1. Since some parts of regions are overlapped one another in the $(\langle r \rangle, \lambda_0)$ plane, regions are shown separately in three figures. Figures 11(a) and (b) show regions of orbits which have positive and negative $\sigma_\parallel$, respectively. Since banana particles take both signs of $\sigma_\parallel$, its region appears on both figures. In figure 11(c), the kidney and concave-kidney regions are shown. To compare with the classification in the (r_s, ξ_s) plane, three characteristic points E (=H), G, and X, which corresponds to the orbits with the same marks in figure 6, are plotted in figure 11.

In the $(\langle r \rangle, \lambda_0)$ plane, these boundaries are obtained by numerical methods. However, in the present configuration with a constant q-value, boundaries *l1* and *l2* in figure 11(a) and (b) can be obtained analytically. These lines correspond to the upper boundary of the outer-circulating region, and the upper boundary of the inner-circulating region which connects to the lower boundary of the banana region, respectively. From equation (19), they are written as

$$\lambda_0 = 2\left(1 \pm \frac{\langle r \rangle}{R_0}\right) \left[1 - \left(\frac{\langle r \rangle}{q\rho}\right)^2 \left(1 - \sqrt{1 - \left(\frac{q\rho}{\langle r \rangle}\right)^2}\right)\right], \tag{39}$$

where we choose $+$ $(-)$ for the boundary *l1* (*l2*). In the limit $\langle r \rangle \gg q\rho$, equation (39) results in $\lambda_0 = 1 \pm \langle r \rangle / R_0$ and agree with the conventional description for the banana region. Because any

orbits on the boundary equation (39) are stagnated on the mid-plane $Z = 0$, their average position are given by $\langle r \rangle = |r_s|$ from equation (19). Then, positions of the points E (=H) is given analytically as

$$[\langle r \rangle, \lambda_0] = \left[(2q^2\rho^2 R_0)^{1/3}, 1 - \frac{9}{4}\left(\frac{q\rho}{2R_0}\right)^{2/3} \right], \quad (40)$$

and the point X is also given as

$$[\langle r \rangle, \lambda_0] = \left[\left(\frac{q^2\rho^2 R_0}{2}\right)^{1/3}, \left\{1 - \left(\frac{q\rho}{4R_0}\right)^{2/3}\right\} \cdot \left\{1 - \frac{1}{2^{1/3}}\left(\frac{q\rho}{R_0}\right)^{2/3}\right\} \right]. \quad (41)$$

To obtain the position of G, which corresponds to the outer-circulating orbit with maximum width $\Delta_{ocmax} = (4q^2\rho^2 R_0)^{1/3}$, we need to calculate its average position numerically. It is given by

$$\mathrm{G}: \qquad [\langle r \rangle, \lambda_0] = \left[\chi (4q^2\rho^2 R_0)^{1/3},\ 1 \right], \quad (42)$$

where the numerical factor is $\chi \simeq 0.58$. We find that χ is almost independent of particle energy and q-value at the axis in the range $0.1\mathrm{keV} < \mathcal{E} < 1\mathrm{MeV}$ and $1 < q < 6$ for ions. The Dependency of regions on particle energy $\mathcal{E}$ and magnetic field configuration appears through $q\rho$ and R_0 in equations (39) to (42). Then, the points E, G, and X move outward in the $\langle r \rangle$-direction for higher energy particles.

There are no particles in the region above the boundary *l1*. In particular, counter-passing and inner-circulating particles, i. e., particles with $\sigma_{\parallel} = -1 = \mathrm{const}$, do not exist in the region above the boundary *l2*. Therefore, there is a limitation on the minimum value of $\langle r \rangle$ for a given $\mathcal{E}$, which is obtained from equation (39) as $\langle r \rangle \geq q\rho$. This is because any particle which passes through the magnetic axis has a finite orbit width.

Overlaps of orbit regions occur around the boundary *l2*. One can see in figure 11(a) and (c) that the upper boundary of the co-passing region *l3* enters the banana region and the gap between *l2* and *l3* corresponds to the kidney region. The kidney region also overlaps with the concave-kidney region, which is enclosed by the solid curve E-G-X in figure 11(c). Such overlaps of regions are caused by the choice of the "radial-like" variable C_3 as $\langle r \rangle$. It is possible that some two orbits, of which orbit topology are different each other, can simultaneously have the same $\mathcal{E}$, μ and $\langle r \rangle$. In contrast to the $(\mathcal{E}, \mu, \langle r \rangle)$ space, overlaps of orbit regions do not occur in the (v, ξ_s, r_s) space, where any set of (v, ξ_s, r_s) corresponds to one definite orbit. The overlap of region in the $(\mathcal{E}, \mu, \langle r \rangle)$ space has not been noticed in the previous works. However, we should take account of these overlaps in Lagrangian formulation of transport theory even if we apply it to the region away from the magnetic axis, because the overlaps between the kidney, co-passing, and banana regions still remain there. To distinguish orbit topology definitely in the $(\mathcal{E}, \mu, \langle r \rangle)$ space, additional information about the number of turning points of $\sigma_{\parallel}$ and σ_{θ} must be retained when we transform Cartesian coordinates to $(\mathcal{E}, \mu, \langle r \rangle)$.

However, there are advantages in using the set of COM $(\mathcal{E}, \mu, \langle r \rangle)$. First, the physical meaning of the flux which is described in the form like equations (6) and (7) with $C_3 = \langle r \rangle$ is more understandable than that with $C_3 = r_s$. In the $(\mathcal{E}, \mu, \langle r \rangle)$ space, particle flux in the $\langle r \rangle$-direction describes the change of average position of particles. And Lagrangian description of transport equations with $(\mathcal{E}, \mu, \langle r \rangle)$ variables has an analogy to the conventional neoclassical transport equations in Eulerian description, in which the magnetic-surface averaged fluxes are given. Second, the change of COM is essentially continuous in the $(\mathcal{E}, \mu, \langle r \rangle)$ space even when a particle crosses boundary *l2*, while r_s changes discontinuously in the (v, ξ_s, r_s) space in that case as pointed out in section 3.1. This is because particles on the boundary *l2* are stagnated at $(r, \theta) = (|r_s|, \pi)$, where r_s satisfies equation (19), and the average radial positions of particles become $\langle r \rangle \to |r_s|$ when they approach the boundary *l2* from both below and above the boundary. Last, any orbit is represented by a point in the $(\mathcal{E}, \mu, \langle r \rangle)$ space, while there are a pair of points for each orbit in the (v, ξ_s, r_s) space.

To describe the diffusion process of particle in the $(\langle r \rangle, \lambda_0)$ plane, the image of particle loci in this plane are illustrated in figures 12(a) and (b), where only the pitch-angle scattering is assumed as the effect of collisions. In figure 12(a), two ion particle loci are shown for the case away from the magnetic axis. One describes the change from co-passing (P+) to banana (B) through kidney (K), and the other is the locus from counter-passing (P−) to banana (B). Note that co-passing particles cannot change into banana particles directly. The diffusion process is more complicated for particles passing near the magnetic axis. In the $(\langle r \rangle, \lambda_0)$ plane, all particles which appear around $\langle r \rangle \sim (q^2\rho^2 R_0)^{1/3}$ and $|\lambda_0 - 1| \sim (q\rho/R_0)^{2/3}$ (the region around the points E (=H), G, and X) have the same characteristic orbit width as potato orbits $\Delta_r \sim \langle r \rangle \sim (q^2\rho^2 R_0)^{1/3}$. In figure 12(b), three loci of ion particles passing through such "potato region" are

shown. A counter-passing particle (P-) enters the concave-kidney region (CK) via the inner-circulating region (IC). There are two ways for a concave-kidney particle to change into banana: (i) It changes into kidney (K) at the boundary G-X first, and then enters the banana region (B) at *l2*, or (ii) directly changes into banana by crossing the boundary G-E. It is also possible for a concave-kidney particle to enter the co-passing region (P+) via the kidney region like the locus (iii).

The rate of the displacement of $\langle r \rangle$ by pitch-angle scattering, which is measured by $\partial\langle r\rangle/\partial\lambda_0$ in the $(\langle r\rangle, \lambda_0)$ plane, is an important factor which indicates the degree of contribution of each type of particle to neoclassical transport. It is convenient to use $\partial\langle\psi\rangle/\partial\mu$ instead of $\partial\langle r\rangle/\partial\lambda_0$ in analysis, since from the conservation of P_ζ, we obtain

$$\frac{\partial\langle\psi\rangle}{\partial\mathbf{v}} = \left(-\frac{I}{\Omega} + \frac{\partial}{\partial v_\parallel}\left\langle\frac{Iv_\parallel}{\Omega}\right\rangle\right)\mathbf{b} = \frac{\partial\langle\psi\rangle}{\partial v_\parallel}\mathbf{b}, \quad (43)$$

and then $\partial\langle\psi\rangle/\partial\mu$ can be written as follows

$$\frac{\partial\langle\psi\rangle}{\partial\mu} = \frac{\partial\mathbf{v}}{\partial\mu}\,\frac{\partial\langle\psi\rangle}{\partial\mathbf{v}} = -\frac{B}{mv_\parallel}\frac{\partial\langle\psi\rangle}{\partial v_\parallel}. \quad (44)$$

It has been shown [7, 9] for particles away from the magnetic axis, that

$$\frac{\partial\langle\psi\rangle}{\partial v_\parallel} \simeq \begin{cases} 0 & : \text{passing particles,} \\ -\dfrac{I}{\Omega_0} & : \text{banana particles.} \end{cases} \quad (45)$$

Therefore, passing particles scarcely change their average position $\langle\psi\rangle$ by collisions and do not contribute to neoclassical transport, except for those very close to the boundaries *l2* or *l3*. We find from numerical calculation of $\partial\langle\psi\rangle/\partial v_\parallel$ that inner-circulating, outer-circulating, kidney, and concave-kidney particles have a finite $\partial\langle\psi\rangle/\partial v_\parallel \sim O(I/\Omega_0)$. Then, not only banana particles but also all types of particle other than passing particles contribute to neoclassical transport described in the $(\mathcal{E}, \mu, \langle r\rangle)$ space. That is the reason why inner- and outer-circulating particles are distinguished from passing particles.

We must pay attention to the change of orbit topology at the boundary *l2*. There are two possibilities for banana particles approaching the boundary *l2* to enter the inner-circulating region or the kidney region. It depends on the position on which the collision makes a banana particle out of the banana region. As shown in figure 13(a), if the collision occurs on the outer part of the banana orbit, then the particle changes into kidney. On the other hand, if the collision occurs on the inner part, it changes into counter-passing. A similar change occurs for concave-kidney particles as in figure 13(b). A concave-kidney particle approaching its lower boundary *l2* (the line E-X in figure 11(c)) changes into kidney or inner-circulating particle according to the position of the last collision. Such bifurcations in change of orbit topology by collisions make particles random walk in the $\langle r\rangle$-direction and cause the neoclassical transport in the $(\mathcal{E}, \mu, \langle r\rangle)$ space.

4. Conclusions

We have investigated in detail the particle motion near the magnetic axis to give a basis of Lagrangian formulation of neoclassical transport theory in this region. Classification of orbit types is made by two sets of constants of motion (COM) (v, ξ_s, r_s) and $(\mathcal{E}, \mu, \langle r\rangle)$, where orbit types are determined by the number of turning points of the signs $\sigma_\parallel = v_\parallel/|v_\parallel|$ and $\sigma_\theta = \dot\theta/|\dot\theta|$ on each orbit. In applying Lagrangian formulation to neoclassical transport theory, it is physically understandable to use the latter set of COM. However, it is found that there are overlaps of regions between different types of orbit in the $(\mathcal{E}, \mu, \langle r\rangle)$ space, and there is a limitation on the minimum value of $\langle r\rangle$ for a given $\mathcal{E}$. These feature must be treated with care when applying Lagrangian representation of transport to the region near the magnetic axis, in which non-standard particle orbits (potato orbits) contribute to neoclassical transport.

References

[1] Stix T H 1972 *Plasma Phys.* **14** 367
[2] Porcelli F, Stankiewicz R, Berk H L and Zhang Y Z 1992 *Phys. Fluids* B **4** 3017
[3] Shaing K C, Hazeltine R D and Zarnstorff M C 1997 *Phys. Plasmas* **4** 771
[4] Shaing K C and Hazeltine R D 1998 *Phys. Plasmas* **5** 953
[5] Helander P 2000 *Phys. Plasmas* **7** 2878
[6] Lin Z, Tang W M and Lee W W 1997 *Phys. Plasmas* **4** 1707
[7] Bernstein I B and Molvig K 1983 *Phys. Fluids* **26** 1488
[8] Zaitsev F S, O'Brien M R and Cox M 1993 *Phys. Fluids* B **5** 509
[9] Wang S 1999 *Phys. Plasmas* **6** 1393
[10] Chu T K 1996 *Phys. Plasmas* **3** 3397
[11] Egedal J 2000 *Nucl. Fusion* **40** 1597
[12] Hinton F L and Hazeltine R D 1972 *Rev. Mod. Phys.* **48** 239

Tables and table captions

Table 1. Classification of particle orbits

orbit type	turning points of $\sigma_{\parallel}$ and σ_{θ}	sign of $\sigma_{\parallel}$	encircle the axis
passing	0 , 0	+ or -	yes
banana	2 , 2	$\pm$	no
outer-circulating	0 , 2	$+^{a}$	no
inner-circulating	0 , 2	$-^{a}$	no
kidney	2 , 0	$\pm$	yes
concave-kidney	2 , 4	$\pm$	yes

[a] For ions The sign is opposite for electrons.

Figure captions

Figure 1. Coordinate system.

Figure 2. Orbits of passing particles. Solid lines represent co-passing orbits ($v_\parallel > 0$) and dashed lines counter-passing orbits ($v_\parallel < 0$). The maximum radial displacement of passing orbit near the axis is shown by the orbit A or C, which is as large as $\sim (q^2\rho^2 R_0)^{1/3}$ However, most of passing orbits have small displacement $\sim 2q\rho$ as shown by the orbits B and D

Figure 3. Orbits of banana particles. The circles and the bars represent the turning points of the sign σ_θ (poloidal angular velocity) and $\sigma_\parallel$ (parallel velocity) respectively. Near the magnetic axis, these two types of turning point tend to deviate from each other The orbit E is the widest banana of which the radial width is Δ_{bmax} given by equation (16).

Figure 4. Orbits of outer-circulating particles (solid lines) and inner-circulating particles (dashed lines). The sign $\sigma_\parallel$ is positive for outer-circulating orbits, while it is negative for inner-circulating orbits Orbits G and H are the widest ones for outer- and inner-circulating orbits, respectively. Inner-circulating orbits exist only in the region enclosed by the orbit H. Outer-circulating orbits can exist away from the magnetic axis like the orbit I.

Figure 5. Orbits of concave-kidney L and kidney M. Only concave-kidney particles have four turning points of σ_θ, while $\sigma_\parallel$ changes twice on both types of orbit.

Figure 6. The regions and the boundaries for each type of orbit in the (r_s, ξ_s) plane, where r_s is the minor radius at which orbits cross the mid-plane $Z = 0$, and $\xi_s = v_\parallel/v$ at that point Negative r_s means the inside of the torus. The regions (i) - (vi) correspond to (i) passing, (ii) banana, (iii) outer-circulating, (iv) inner-circulating, (v) concave-kidney, and (vi) kidney, respectively. Dotted lines given by equation (19) in the circulating regions correspond to circulating particles with $r = \dot{\theta} = 0$. Dash-dotted lines *b1* are given by equation (20). Solid line *b2* enclosing the region (ii) is given by equation (26). Dashed line *b3* is given by equation (27). Pairs of the same marks B, D, etc. correspond to the orbits in figures 2 - 5 (See also figures 7 and 8 for some orbits not shown here.)

Figure 7. A magnification of the region near the origin in the (r_s, ξ_s) plane in figure 6. Pairs of marks correspond to the orbits in figures 2 – 5.

Figure 8. The regions of concave-kidney (v) and kidney (vi) at $r_s > 0$. The boundary G-X between these two regions plotted by the dotted line is given by equation (25). Other lines and marks are defined in the same way as in figure 6.

Figure 9. Orbital integrations along inner- and outer-circulating particle orbits. The circles and $\pm$ represent turning points and signs of σ_θ, respectively. For a given $(\mathcal{E}, \mu, \langle r \rangle)$, there are two solutions for the particle position $r(\theta)$ which are distinguished by $\sigma_\theta = \pm 1$.

Figure 10. Orbital integration along a concave-kidney particle orbit. The bars represents the turning points of $\sigma_\parallel$, and other marks are used in the same meaning as in figure 9

Figure 11. The regions and the boundaries for each type of orbit in the $(\langle r \rangle, \lambda_0)$ plane, where $\langle r \rangle$ is bounce-averaged minor radius of particles, and $\lambda_0 = \mu B_0/\mathcal{E}$ is the normalized magnetic moment. Figures (a) and (b) show the regions for orbits with $\sigma_\parallel = +1$ and $\sigma_\parallel = -1$, respectively. The kidney region (the shaded region) and the concave-kidney region (enclosed by the boundary E-G-X) are shown in figure (c). There is an overlap of orbit regions between co-passing and banana orbits in figure (a) (the shaded region). As shown in Fig (c), the kidney region overlaps with the co-passing, banana, and concave-kidney regions. No particles can exist in the region above the boundary *l1*.

Figure 12. Particle loci (for case of ions) in the $(\langle r \rangle, \lambda_0)$ plane Orbit types are abbreviated as P+; co-passing, P-; counter-passing, K; kidney, B; banana, CK; concave-kidney, and IC; inner-circulating orbits, respectively. The change in orbit types for particles away from the magnetic axis is shown in figure (a), while figure (b) shows the change for particles passing near the axis, that is, for potato particles. In the $(\langle r \rangle, \lambda_0)$ plane, particle loci are essentially continuous on the boundaries of orbit types.

Figure 13. The change in orbit topology. (a) A banana orbit change into a kidney orbit or a counter-passing orbit according to the position on which the last collision occurs. (b) Similarly, a concave-kidney changes into a kidney orbit or an inner-circulating orbit.

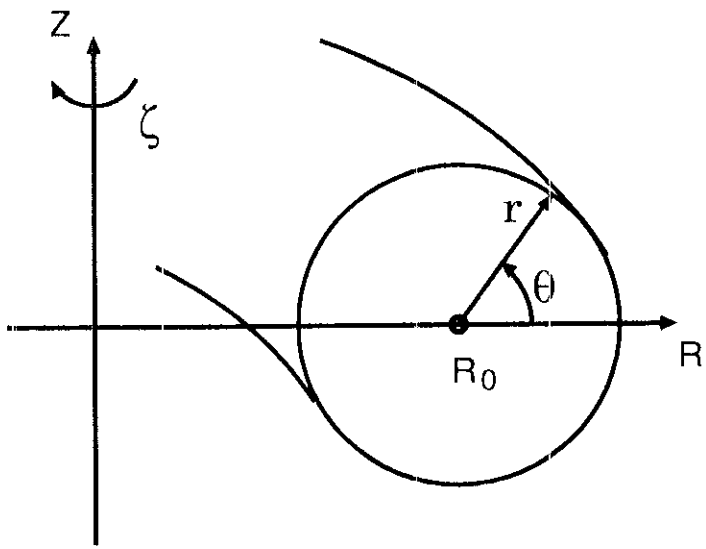

figure 1

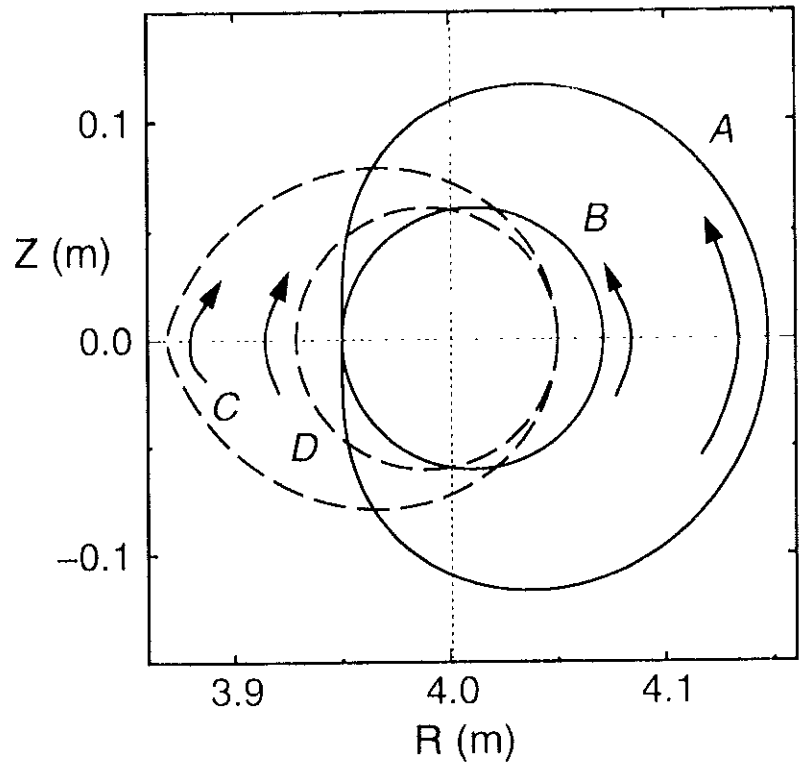

figure 2

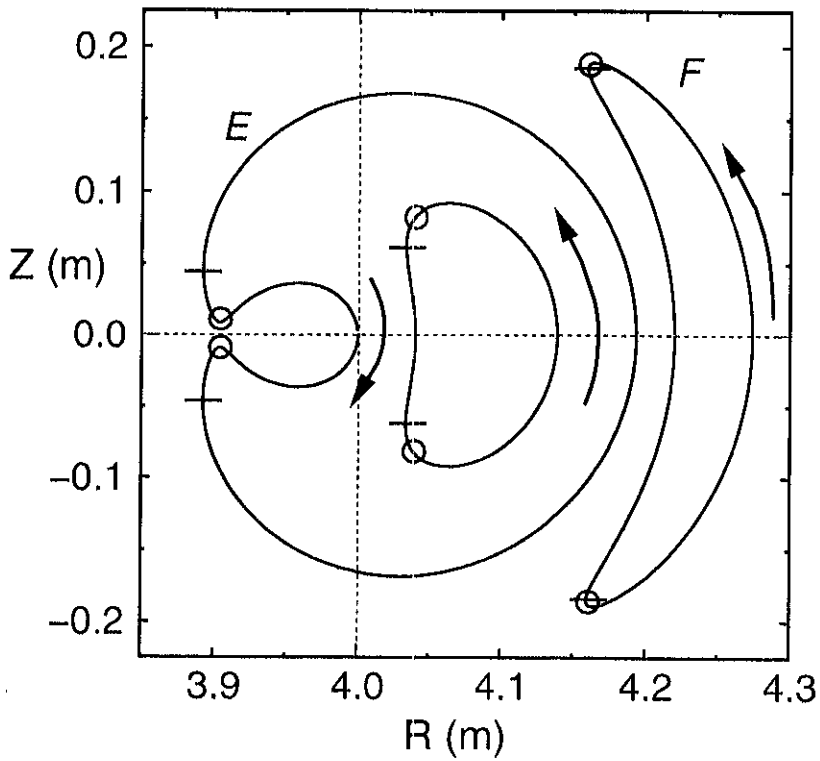

figure 3

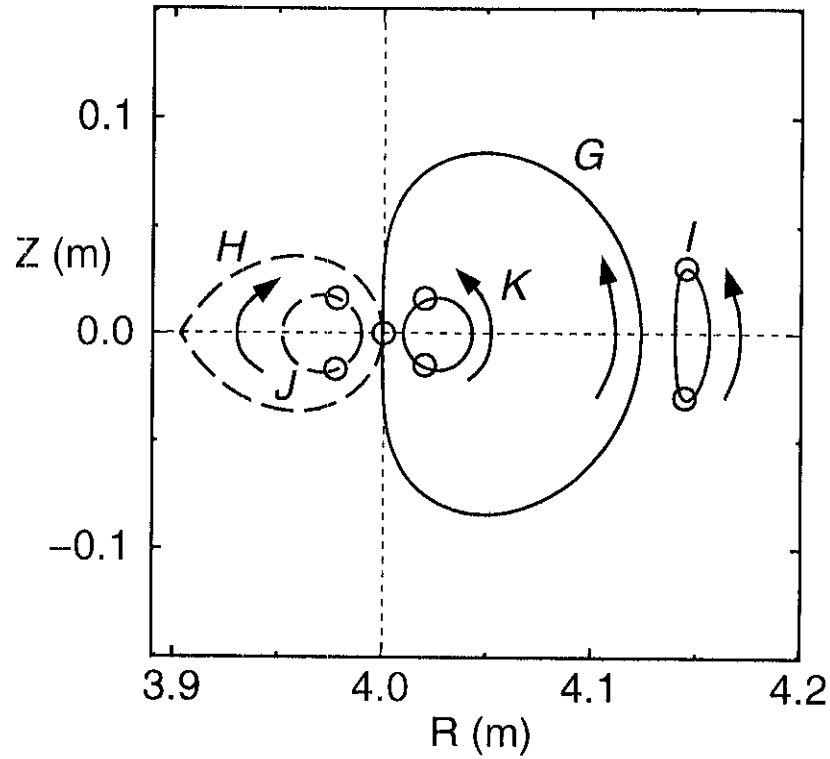

figure 4

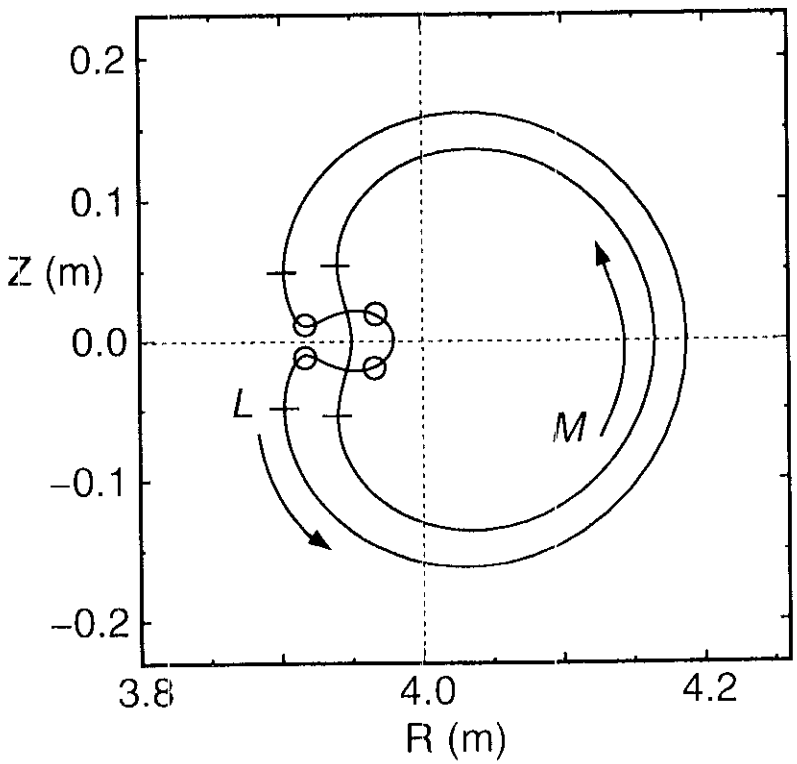

figure 5

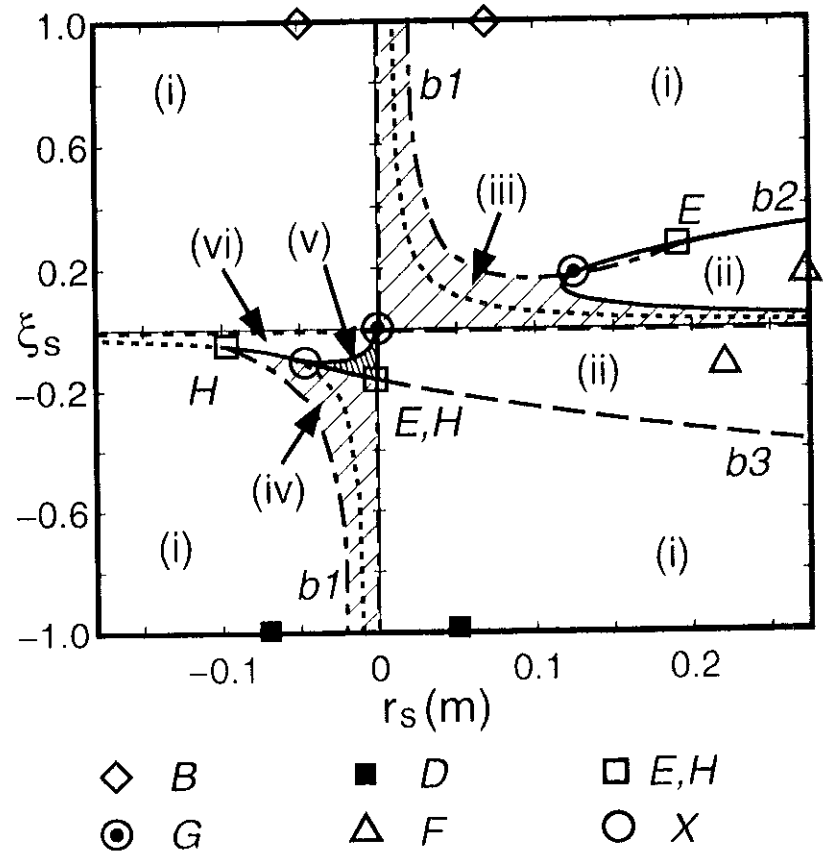

figure 6

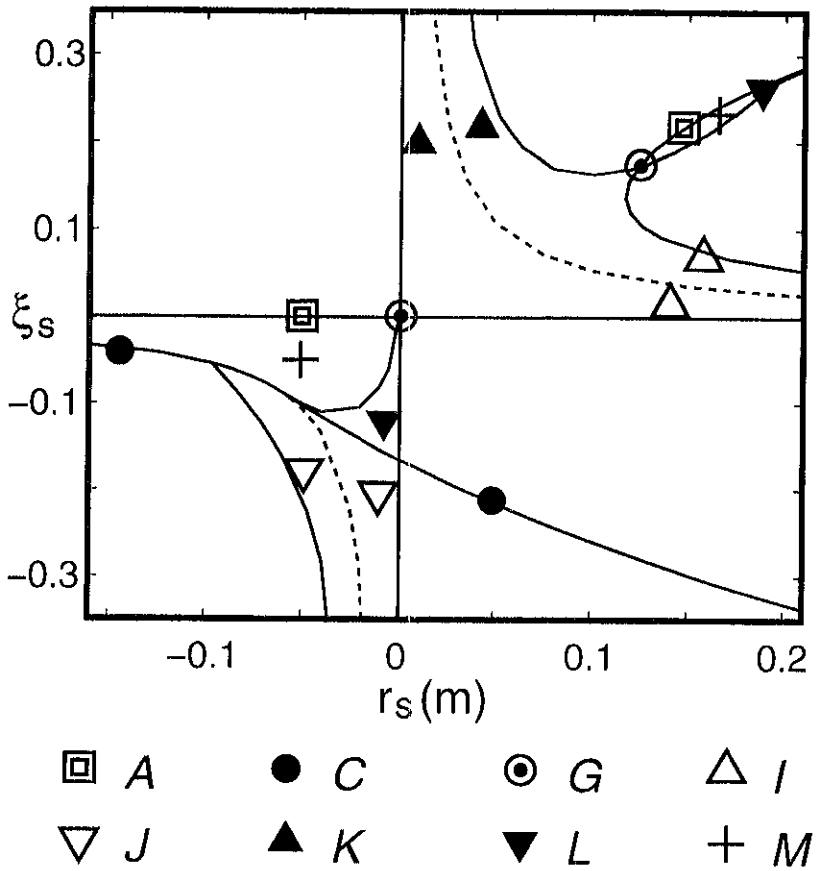

figure 7

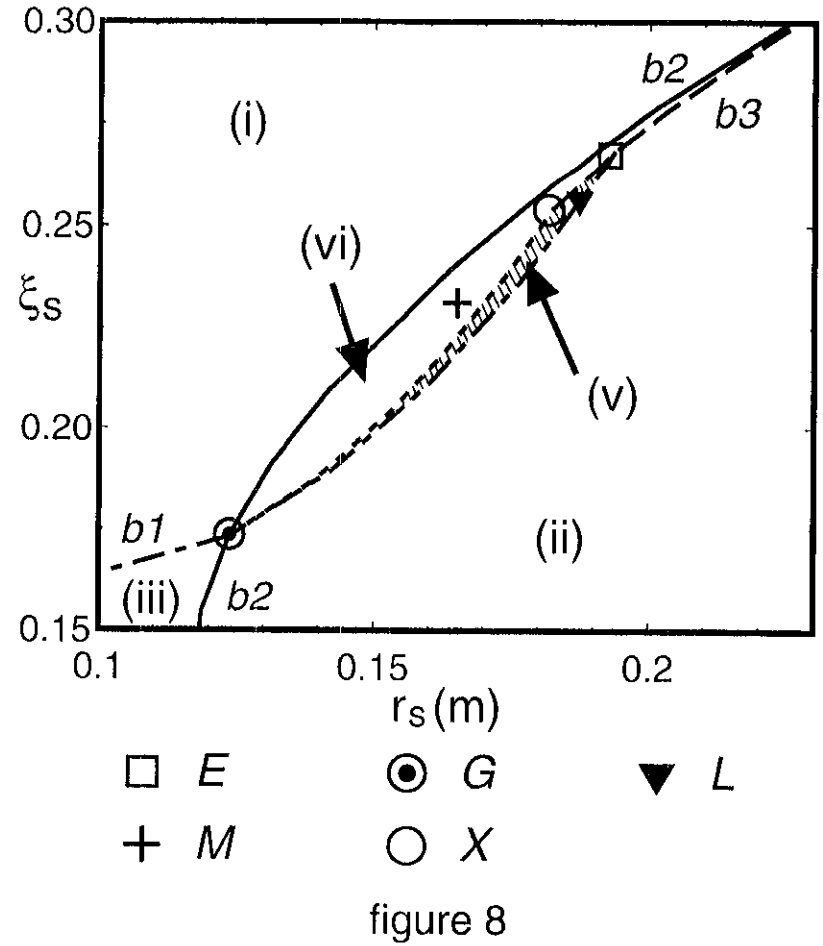

figure 8

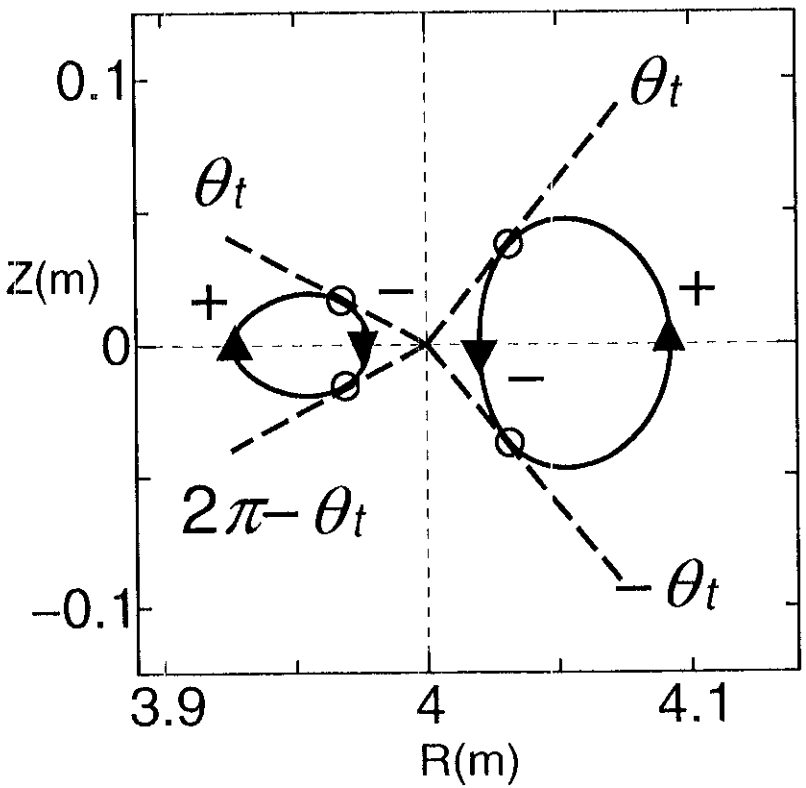

figure 9

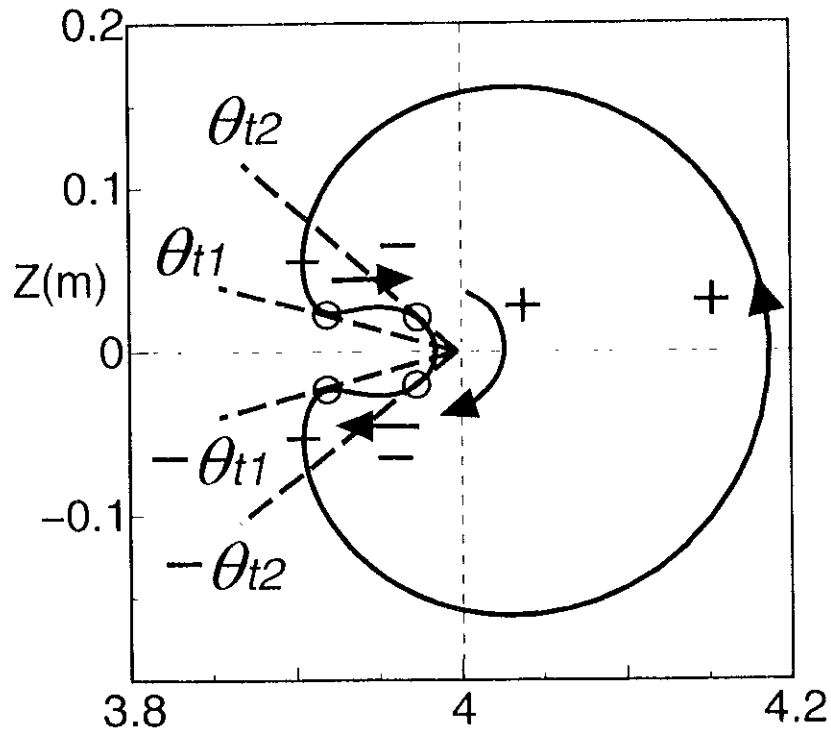

figure 10

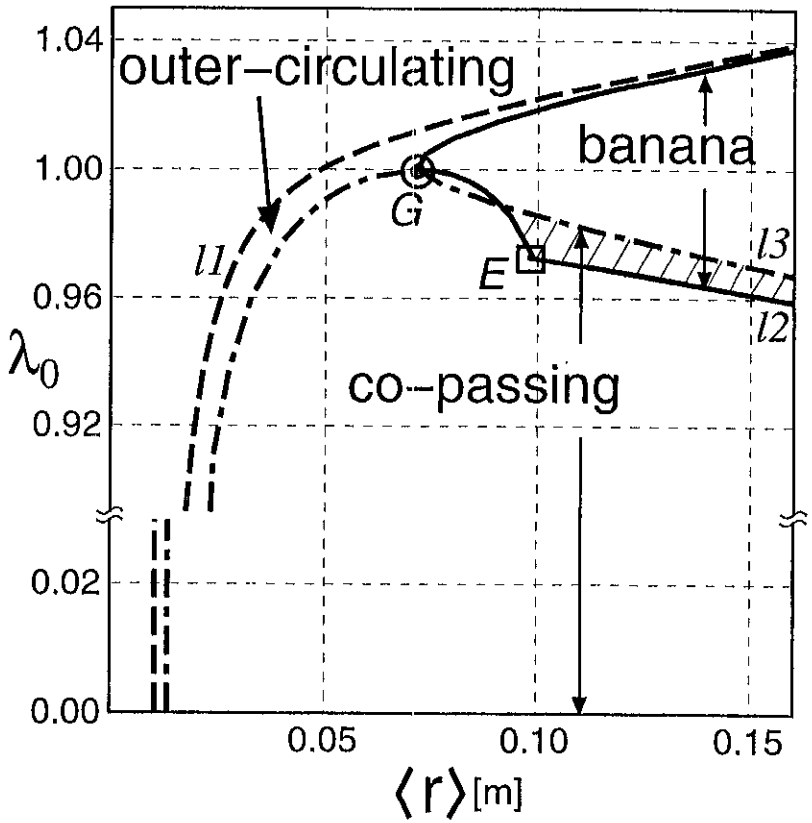

figure 11(a)

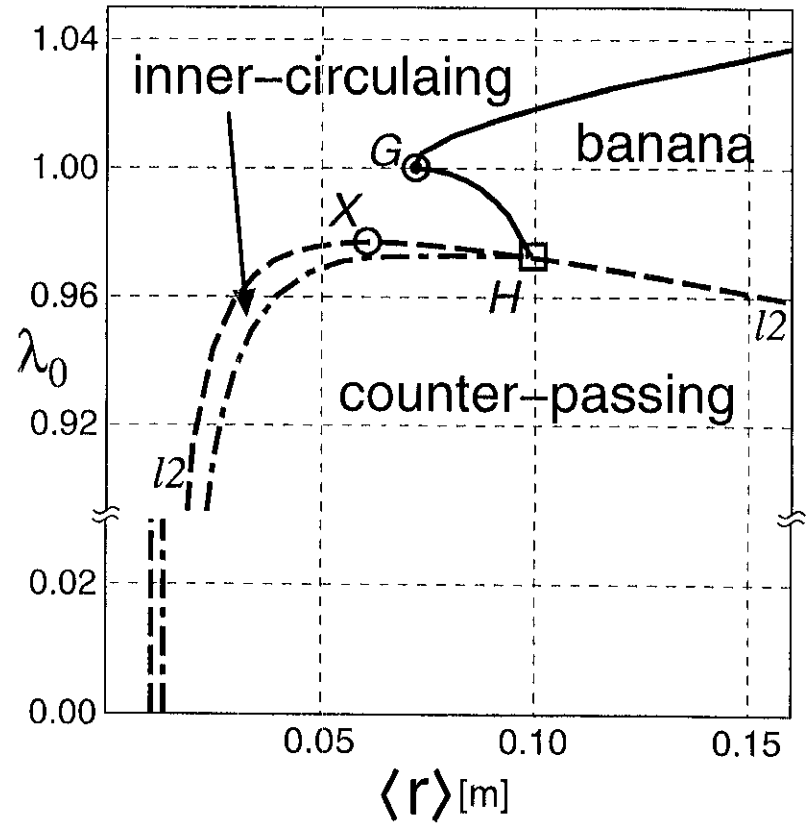

figure 11(b)

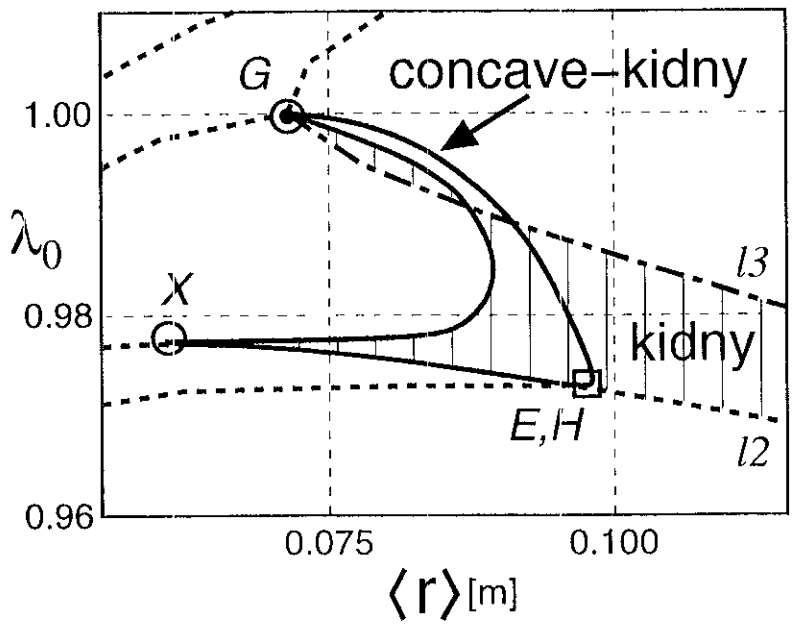

figure 11(c)

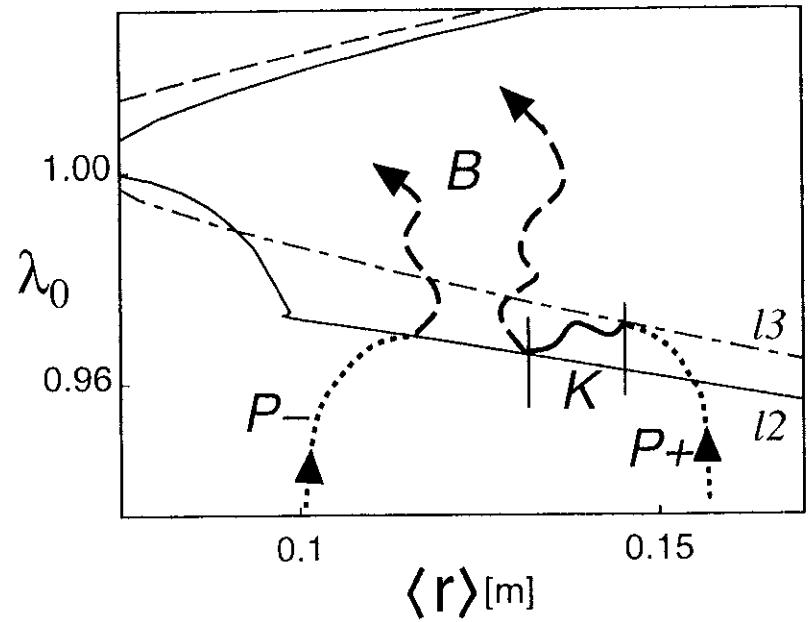

figure12a

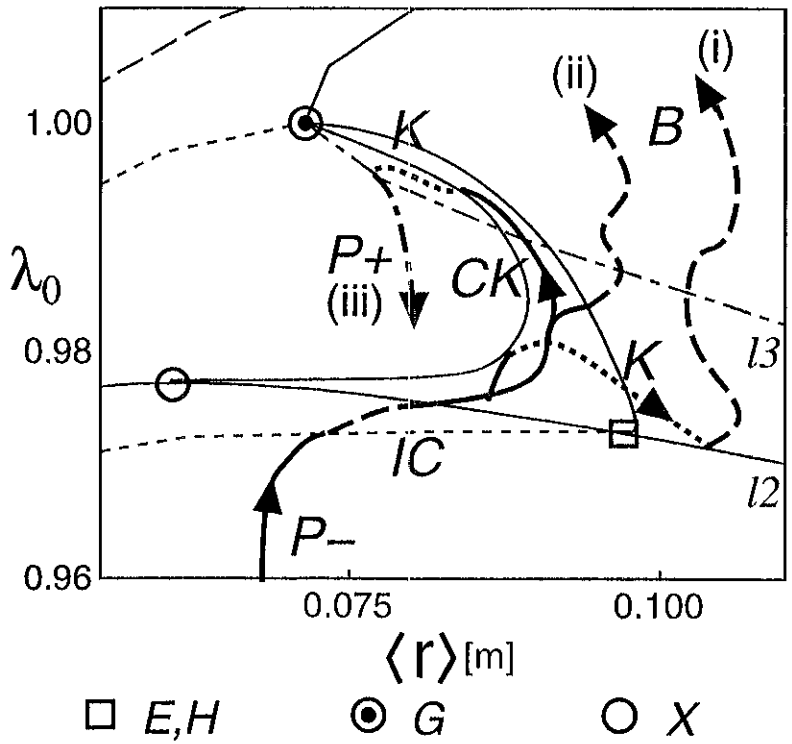

figure12b

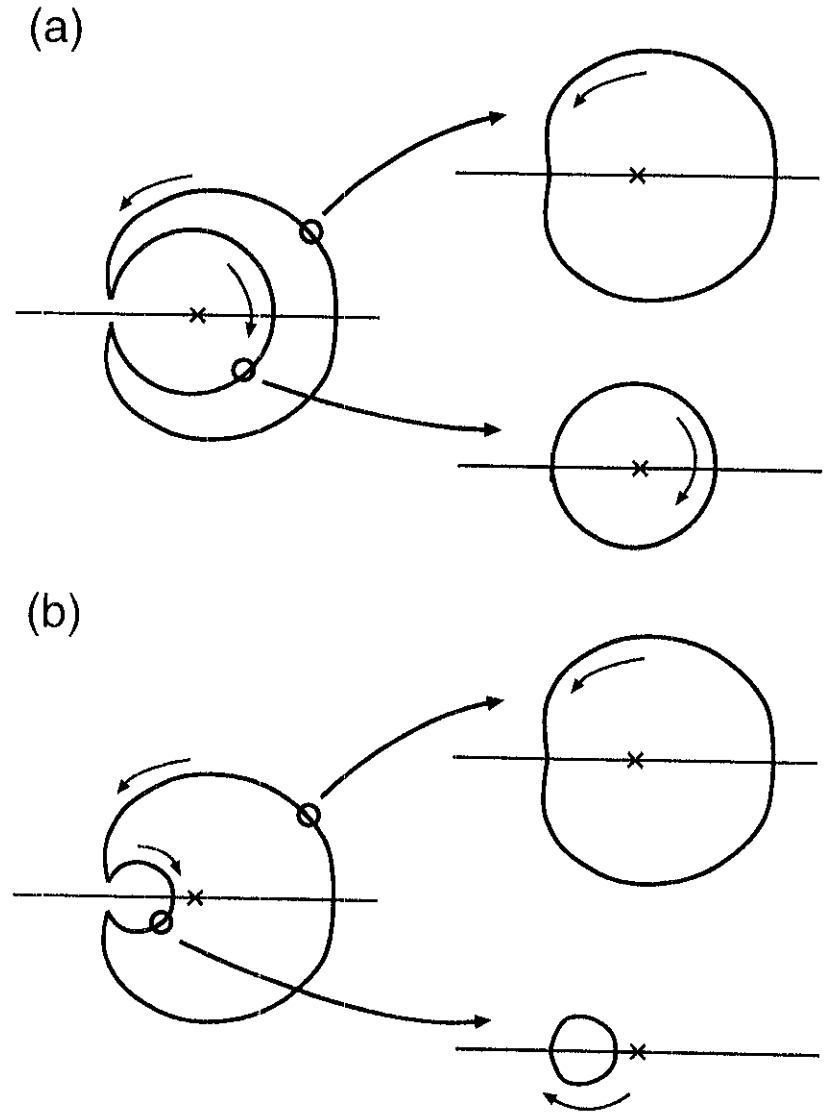

figure 13

Recent Issues of NIFS Series

NIFS-659 T Satow, S Imagawa, N Yanagi, K Takahata, T Mito, S Yamada, H Chikaraishi, A Nishimura, I Ohtake, Y Nakamura, S Satoh, O Motojima,
Achieved Capability of the Superconducting Magnet system for the Large Helical Device, Sep. 2000
(IAEA-CN-77/FTP1/15)

NIFS-660 T Watari, T Mutoh, R Kumazawa, T Seki, K Saito, Y Torii, Y P Zhao, D Hartmann, H Idei, S Kubo, K Ohkubo, M Sato, T Shimozuma, Y Yoshimura, K Ikeda, O Kaneko, Y Oka, M Osakabe, Y Takeiri, K Tsumori, N Ashikawa, P C deVries, M Emoto, A Fukuyama, H Funaba, M Goto, K Ida, S Inagaki, N Inoue, M Isobe, K Itoh, S Kado, K Kawahata, T Kobuchi, K Khlopenkov, A Komori, A Krasilnikov, Y Liang, S Masuzaki, K Matsuoka, T Minami, J Miyazawa, T Morisaki, S Morita, S Murakami, S Muto, Y Nagayama, Y Nakamura, H Nakanishi, K Narihara, K Nishimura, N Noda, A TNotake, S Ohdachi, N Ohyabu, H Okada, M Okamoto, T Ozaki, R O Pavlichenko, B J Peterson, A Sagara, S Sakakibara, R Sakamoto, H Sasao, M Sasao, K Sato, S Satoh, T Satow, M Shoji, S Sudo, H Suzuki, M Takechi, N Tamura, S Tanahashi, K Tanaka, K Toi, T Tokuzawa, K Y Watanabe, T Watanabe, H Yamada, I Yamada, S Yamaguchi, S Yamamoto, K Yamazaki, M Yokoyama, Y Hamada, O Motojima, M Fujiwara,
The Performance of ICRF Heated Plasmas in LHD, Sep. 2000
(IAEA-CN-77/EX8/4)

NIFS-661 K Yamazaki, K Y Watanabe, A Sagara, H Yamada, S Sakakibara, K Narihara, K Tanaka, M Osakabe, K Nishimura, O Motojima, M Fujiwara, the LHD Group,
Helical Reactor Design Studies Based on New Confinement Scalings, Sep. 2000
(IAEA-CN-77/ FTP 2/12)

NIFS-662 T Hayashi, N Mizuguchi, H Miura and T Sato,
Dynamics of Relaxation Phenomena in Spherical Tokamak, Sep. 2000
(IAEA-CN-77THP2/13)

NIFS-663 H Nakamura and T Sato, H Kambe and K Sawada and T Saiki,
Design and Optimization of Tapered Structure of Near-field Fiber Probe Based on FDTD Simulation, Oct. 2000

NIFS-664 N Nakajima,
Three Dimensional Ideal MHD Stability Analysis in $L=2$ Heliotron Systems, Oct. 2000

NIFS-665 S Fujiwara and T Sato,
Structure Formation of a Single Polymer Chain I Growth of trans Domains, Nov. 2000

NIFS-666 S. Kida,
Vortical Structure of Turbulence, Nov. 2000

NIFS-667 H Nakamura, S Fujiwara and T Sato,
Rigidity of Orientationally Ordered Domains of Short Chain Molecules, Nov. 2000

NIFS-668 T Mutoh, R Kumazawa, T Seki, K Saito, Y Torii, F Shimpo, G Nomura, T Watari, D A Hartmann, M Yokota, K Akaishi, N Ashikawa, P deVries, M Emoto, H Funaba, M Goto, K Ida, H Idei, K Ikeda, S Inagaki, N Inoue, M Isobe, O. Kaneko, K Kawahata, A Komori, T Kobuchi, S Kubo, S Masuzaki, T Morisaki, S Morita, J Miyazawa, S Murakami, T Minami, S Muto, Y Nagayama, Y Nakamura, H Nakanishi, K Narihara, N Noda, K Nishimura, K Ohkubo, N Ohyabu, S Ohdachi, Y Oka, M Osakabe, T Ozaki, B J Peterson, A Sagara, N Sato, S Sakakibara, R Sakamoto, H Sasao, M Sasao, M Sato, T Shimozuma, M Shoji, S Sudo, H Suzuki, Y Takeiri, K Tanaka, K Toi, T Tokuzawa, K Tsumori, K Y Watanabe, T Watanabe, H Yamada, I Yamada, S Yamaguchi, K Yamazaki, M Yokoyama, Y Yoshimura, Y Hamada, O Motojima, M Fujiwara,
Fast- and Slow-Wave Heating of Ion Cyclotron Range of Frequencies in the Large Helical Device, Nov. 2000

NIFS-669 K Mima, M S Jovanovic, Y Sentoku, Z-M. Sheng, M M Skoric and T Sato,
Stimulated Photon Cascade and Condensate in Relativistic Laser-plasma Interaction, Nov. 2000

NIFS-670 L Hadzievski, M M Skoric and T Sato,
On Origin and Dynamics of the Discrete NLS Equation, Nov. 2000

NIFS-671 K Ohkubo, S Kubo, H Idei, T Shimozuma, Y Yoshimura, F Leuterer, M Sato and Y Takita,
Analysis of Oversized Sliding Waveguide by Mode Matching and Multi-Mode Network Theory, Dec. 2000

NIFS-672 C Das, S. Kida and S Goto,
Overall Self-Similar Decay of Two-Dimensional Turbulence, Dec. 2000

NIFS-673 L.A Bureyeva, T Kato, V.S. Lisitsa and C Namba,
Quasiclassical Representation of Autoionization Decay Rates in Parabolic Coordinates, Dec. 2000

NIFS-674 L A Bureyeva, V.S Lisitsa and C. Namba,
Radiative Cascade Due to Dielectronic Recombination, Dec. 2000

NIFS-675 M FHeyn, S V Kasilov, W Kernbichler, K Matsuoka, V V Nemov, S Okamura, O S Pavlichenko,
Configurational Effects on Low Collision Plasma Confinement in CHS Heliotron/Torsatron, Jan. 2001

NIFS-676 K. Itoh,
A Prospect at 11th International Toki Conference - Plasma physics, quo vadis?, Jan. 2001

NIFS-677 S Satake, H Sugama, M Okamoto and M Wakatani,
Classification of Particle Orbits near the Magnetic Axis in a Tokamak by Using Constants of Motion, Jan. 2001